arXiv:2605.22183v2 [cs.RO] 24 May 2026

Action with Visual Primitives

Weilong Guo*†‡
Anyverse Dynamics
weilong.guo@anyverse.com

Yuchen Wang*
Tsinghua University
wyuchen0416@zju.edu.cn

Renping Zhou
Tsinghua University
zrp21@mails.tsinghua.edu.cn

Yunfeng Zhang
Anyverse Dynamics
yunshan.zhang@anyverse.com

Rui Fang
Anyverse Dynamics
rui.fang@anyverse.com

Yuyang Pang
Anyverse Dynamics
yuyang.pang@anyverse.com

Wenda Xu‡
Anyverse Dynamics
wenda.xu@anyverse.com

Gao Huang‡
Tsinghua University
gaohuang@tsinghua.edu.cn

Project page: https://kingdroper.github.io/AVP

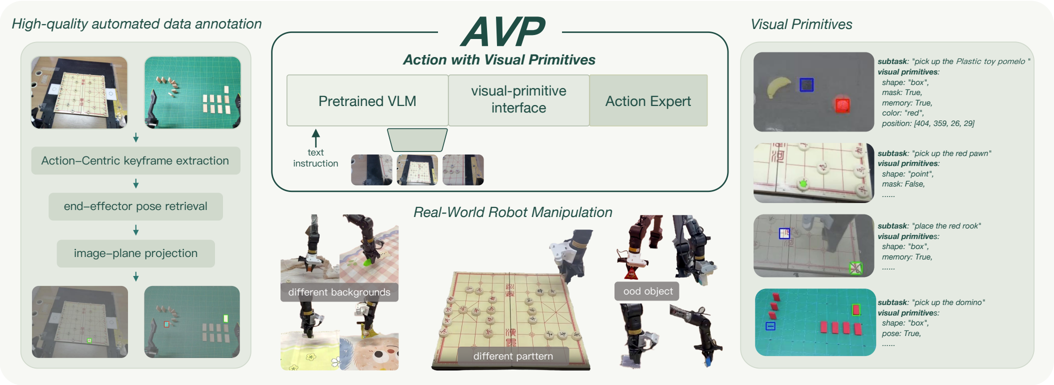

Figure 1: We present AVP, an end-to-end Vision-Language-Action architecture with a visual-primitive interface. The VLM infers the next-stage target and emits spatially grounded visual-primitive tokens, which condition a action expert to execute real-world robot manipulation tasks. Visual-primitive supervision is derived directly from end-effector kinematics, avoiding manual spatial annotation or external visual prompt generators.

Abstract: Vision-Language-Action (VLA) models have emerged as a promising paradigm for generalist robotic manipulation. A common design in current architectures maps language instructions and visual observations to actions in a single forward pass. While conceptually simple, this formulation entangles instruction comprehension, spatial scene understanding, and motor control within a single learning objective. As a result, the action expert must implicitly relearn cognitive and perceptual capabilities already present in the pretrained VLM, which can limit both learning efficiency and generalization. We introduce AVP (Action with Visual Primitives), an end-to-end architecture that implements this visual-primitive-centric interface: the VLM infers the next-stage target and emits visual-primitive tokens that condition a flow-matching action expert, with supervision

---

[*] Equal contribution.
[†] Project Leader.
[‡] Corresponding author.

derived from end-effector kinematics. Real-robot experiments on general pick-and-place tasks show that AVP improves the success rate by 27.61% over $\pi_{0.5}$ and outperforms other recent methods, with consistent gains in data efficiency, spatial-compositional generalization, and object-level transfer.

Keywords: Vision-Language-Action, Visual Primitives, Robotic Manipulation, End-to-End

1 Introduction

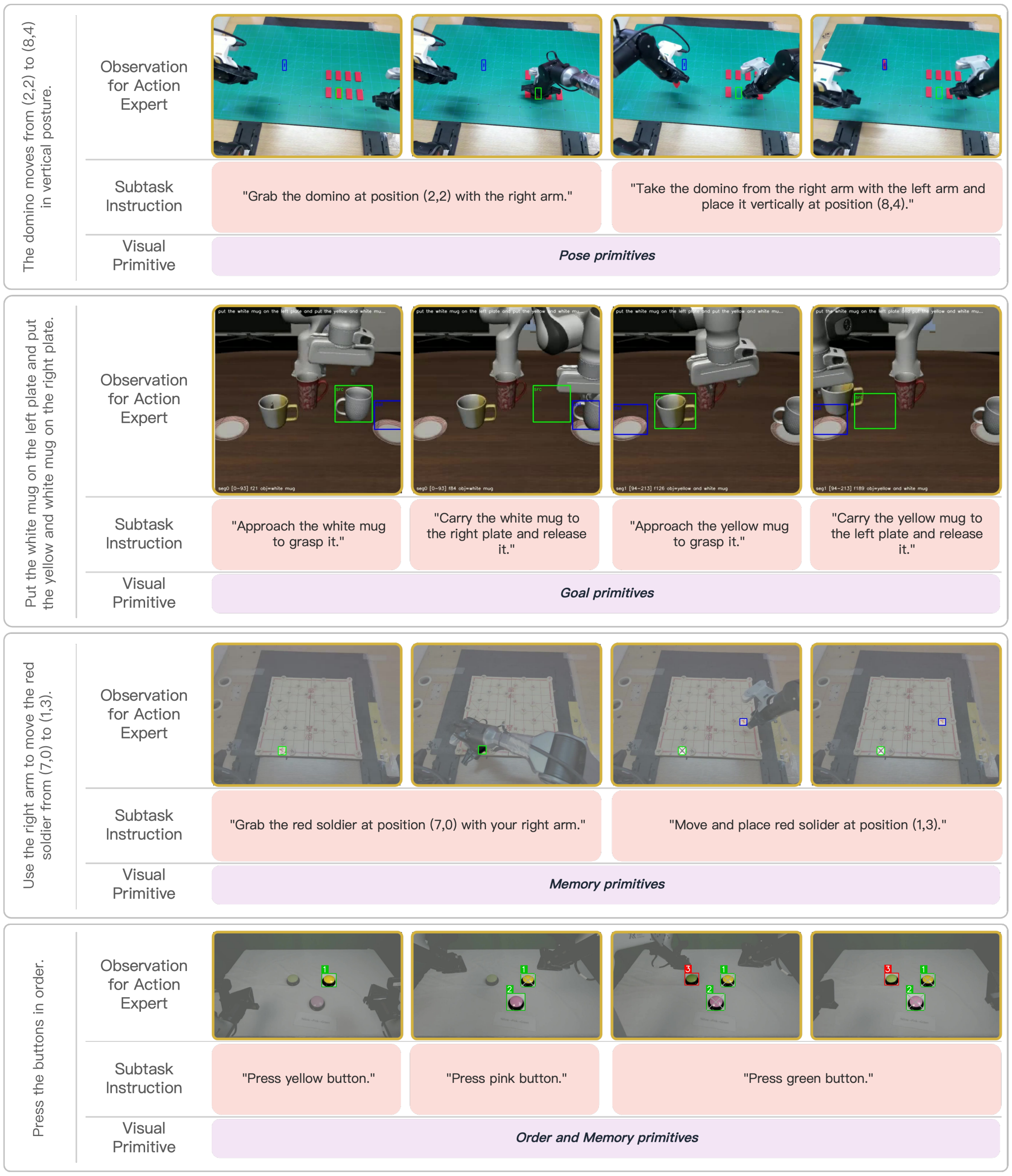

Figure 2: **Different visual primitives of our AVP.**

Building general-purpose robots that perform diverse manipulation tasks in the open world is a long-standing goal of embodied AI. Inspired by the success of large pre-trained models in language and vision, recent research has introduced Vision-Language-Action (VLA) models [1, 2, 3, 4, 5], which fine-tune Vision-Language Models on large-scale robotic datasets [6, 7, 8, 9] to unify language understanding, visual perception, vision-language alignment, and action generation in a single framework. Pioneering works such as RT-2 [10], OpenVLA [1], and $\pi_{0.5}$ [3] have demonstrated this paradigm's effectiveness across a variety of complex multi-task scenarios.

However, existing VLA architectures have yet to fully leverage the semantic and spatial reasoning capabilities that VLMs acquire through large-scale pre-training. A central challenge is that current designs require the action expert to map raw VLM features directly to motor commands, mixing perception, reasoning, and control within a single learning objective [11, 12, 13]. This coupling makes it hard for the action expert to separate transferable motor skills from task-specific visual context, which often shows up as weak generalization when objects, layouts, or environments change at test time. Several lines of work seek to address this by introducing explicit intermediate representations. **(i)** Planning-centric approaches [3, 14, 15] such as $\pi_{0.5}$ break instructions into *subtask descriptions*, letting the action expert focus on atomic motor skills and thereby improving compositional generalization. Still, the interface remains purely linguistic and can struggle to convey fine-grained spatial distinctions, especially in visually dense scenes or among geometrically similar entities. **(ii)** $\pi_{0.7}$ [16] and world-action models [17, 18] provide *subgoal images* or predicted future frames as a visual target for the action expert. While spatially informative, dense pixel predictions still require the action expert to re-discover what in the scene actually matters for the task. **(iii)** Visual-prompt methods such as Point-VLA [19], VP-VLA [20] and TraceVLA [21] turn VLM outputs into spatial markers drawn on the input image, offering direct spatial grounding. However, these approaches rely on external models to produce the prompts, leading to multi-stage pipelines that add inference latency and risk passing errors from one stage to the next.

This motivates us to revisit a fundamental question: *how should responsibilities be partitioned between the VLM and the action expert?* Ideally, the two should function as a cohesive whole yet maintain a clear division of learning responsibilities—the VLM reasons about what to do and where, while the action expert focuses solely on how to execute. Building on these observations, we propose **AVP (Action with Visual Primitives)**, an end-to-end VLA architecture that places visual communication at the center of the VLM↔action-expert boundary. AVP explicitly demarcates the learning responsibilities of the two modules through a *visual-primitive-centric communication protocol*: the VLM emits visual primitives—points, bounding boxes, or any of the forms exemplified in fig. 2—that the action expert reads as direct, visually grounded instructions to execute. Our AVP consists of three components: a pretrained VLM, an autoregressive decoder, and an action expert. Given a language instruction and multi-view observations of the robot, the VLM parses the current subtask and predicts both the next-stage target and the visual primitives used to represent it. This latent prediction is then projected from the language space into the visual space, yielding image tokens overlaid with visual primitives. These tokens, in turn, serve as the condition that drives the action expert to produce robot actions. Such a design is both simple and expressive. It offloads complex spatial reasoning from the action expert, implicitly encodes world-model-like predictions of future states, and extends naturally to memory-augmented variants.

Through real-world robot experiments, we demonstrate that AVP achieves strong manipulation performance across multiple tasks, including Chinese chess manipulation, domino placement, and general object pick-and-place. Beyond standard task execution, AVP exhibits strong spatial compositional generalization, enabling direct execution of unseen transitions, as well as effective zero-shot generalization to unseen objects. Under identical experimental conditions, our method improves the overall manipulation success rate by 27.61% over the $\pi_{0.5}$ baseline.

In summary, our contributions are as follows:

- We revisit the division of responsibilities between the VLM and the action expert, and propose visual primitives—spatially grounded tokens produced internally by the VLM—as an explicit communication medium that replaces the implicit, unstructured boundary in current VLAs.
- We introduce AVP, which implements this idea end-to-end: the VLM infers the next-stage target and emits visual-primitive tokens that condition a flow-matching action expert, with supervision derived from end-effector kinematics.

- Experiments on multiple real-robot pick-and-place tasks show a 27.61% success-rate improvement over $\pi_{0.5}$, along with meaningful gains in spatial-compositional and object-level generalization.

2 Related Work

Vision-Language-Action Models. Vision-Language-Action (VLA) models unify visual, language, and action modalities into a single policy, emerging as a practical paradigm for robotic control [22, 23, 4, 2, 24, 5]. By leveraging the inherent comprehension capabilities of Large Language Models (LLMs) and Vision-Language Models (VLMs), and pre-training on large-scale, heterogeneous multimodal datasets, current VLAs demonstrate strong transferability and generalization across diverse tasks. Previous works such as RT-2 [10], and OpenVLA [1] have explored the feasibility and scaling behavior of training on large scale robot datasets. Recent advancements, such as $\pi_{0.5}$ [3] and GR-3 [25], have further enhanced the robustness of action policies and real-world deployment efficacy by incorporating flow-matching action experts [26, 27]. Building upon this line of work, cutting-edge generalist architectures like DM0 [28] and LDA [29] push the limits of physical AI through embodied-native training recipes or joint multi-objective latent dynamics optimization. However, although existing VLAs exhibit basic spatial understanding and grounding capabilities derived from their VLM backbones, they often lack sufficient spatial reasoning proficiency when guided by complex natural language instructions [30, 31, 32]. Consequently, a significant gap persists between high-level language directives and the precise low-level visual observations required for fine-grained execution.

Visual Prompting as Intermediate Representations for VLAs. Intermediate visual representations play a crucial role in guiding robotic behavior and facilitating complex control tasks. Existing methods usually employ auxiliary pre-trained vision models—such as the Segment Anything Model (SAM) [33, 34] or generic VLMs [35, 36, 37]—to ground natural language instructions into explicit visual markers directly on the input image, utilizing formats like key points [38, 39, 40], bounding boxes [20, 19, 41], masks [42, 43] and trajectories [44, 45, 21]. Although such structured spatial prompting enhances scene understanding and spatial localization capabilities in complex environments, this cascaded, dual-system architecture inherently introduces compounded precision errors and significant execution latency. Furthermore, the generation of these visual markers often relies on task-specific, heuristic designs, which severely limits their scalability across tasks and environments. Our approach overcomes these critical limitations by modeling visually prompted images at the discrete visual token level. Through an end-to-end co-optimization framework, we successfully internalize the spatial reasoning capabilities of pre-trained vision models directly into the VLA policy, entirely bypassing the overhead and fragility of external modular dependencies.

3 Method

3.1 VLA Policies and Cascaded Visual Prompting

Typical Vision-Language-Action (VLA) models [4, 3, 25] characterize robotic manipulation as a direct mapping $a_{t:t+h} = \pi_\theta(o_t, l, s_t)$ to predict an action horizon h conditioned on visual observation o_t, a language instruction l, and proprioceptive state s_t. However, this direct formulation establishes only an implicit interface between high-level understanding and low-level execution, where task-relevant spatial primitives remain entangled within global features. As a result, the policy must jointly learn semantic grounding, spatial localization, and motion generation, leading to low data efficiency and poor generalization under spatial or layout shifts.

To mitigate this, alternative paradigms introduce cascaded visual prompting [20, 21] to explicitly factorize perception and control into a two-stage pipeline. Formally, a task-conditioned perception module $\mathcal{M}_{per}$ first extracts an explicit visual prompt v_t (e.g., coordinate points or bounding boxes). This prompt is then visually fused onto the original observation to guide a downstream action policy π_{act}:

$$v_t = \mathcal{M}_{per}(o_t, l), \quad \text{and} \quad a_{t:t+h} = \pi_{act}(\mathcal{F}(o_t, v_t), l, s_t), \tag{1}$$

where $\mathcal{F}(\cdot)$ denotes a visual composition operator (e.g., pixel-level overlaying or rendering). Although this cascaded formulation unburdens the action policy from spatial localization, it relies on decoupled, non-end-to-end architectures that introduce non-negligible inference latency and suffer from cascading error propagation across stages.

3.2 AVP: Action with Visual Primitives

Building on these observations, we introduce AVP, which uses visual primitives as an explicit interface between high-level understanding and low-level execution. AVP consists of three components: a VLM, a visual-primitive decoder, and an action expert. Unlike cascaded visual prompting methods that rely on external perception modules, AVP internalizes this interface within a single end-to-end VLA model, thereby decoupling spatial grounding from action generation without introducing a fragmented pipeline.

Given the instruction l and observation o_t, the VLM produces multimodal context tokens, from which the visual-primitive decoder autoregressively predicts a discretized visual primitive for the next stage of execution:

$$p_t = D_\psi(\mathrm{VLM}(o_t, l)). \tag{2}$$

The predicted primitive p_t encodes the next-stage subtask together with its associated spatial target, and serves as the explicit condition for subsequent action prediction. To make this interface directly consumable by the action expert, we project the predicted primitive into the visual token space:

$$z_t^{vp} = \mathrm{Proj}(p_t, o_t), \tag{3}$$

where z_t^{vp} denotes the projected visual-primitive tokens. These tokens are then fused with the original multimodal tokens to form an augmented multimodal representation z_t^{aug}, which is used by the action expert for action prediction:

$$a_{t:t+h} = \pi_\theta(z_t^{aug}, s_t). \tag{4}$$

Through this design, the visual primitive acts as an explicit communication channel between the VLM and the action expert: the VLM specifies the task-relevant target in the visual space, while the action expert focuses on motion execution.

We supervise the visual-primitive decoder with an auxiliary visual-primitive prediction loss:

$$\mathcal{L}_{vp} = \mathcal{L}_{CE}\big(p_t, y_t^{vp}\big), \tag{5}$$

where y_t^{vp} denotes the ground-truth visual primitive derived from end-effector kinematics. The action expert is trained with the standard action prediction objective $\mathcal{L}_{act}$, and the overall training objective is

$$\mathcal{L} = \mathcal{L}_{act} + \lambda \mathcal{L}_{vp}, \tag{6}$$

where λ balances action learning and primitive supervision.

At inference time, AVP requires only the raw observation, language instruction, and robot state. Visual primitives are generated internally without any external detector, segmenter, or manually overlaid prompt.

3.3 Action-Centric Visual-Primitive Supervision

Primitive supervision is derived directly from end-effector kinematics, eliminating the need for manual spatial annotation or external visual prompt generators. Specifically, we construct supervision in three steps: keyframe extraction, end-effector pose retrieval, and image-plane projection. We first identify interaction keyframes from gripper-state transitions. At each keyframe, we extract the corresponding 3D end-effector position from robot proprioception and project it into each camera view to obtain 2D spatial anchors. These anchors are then discretized into visual-primitive labels for training the decoder.

This kinematics-guided pipeline provides supervision that is directly tied to robot interaction while introducing little additional annotation cost beyond standard real-robot demonstrations. Full details are provided in Appendix B.

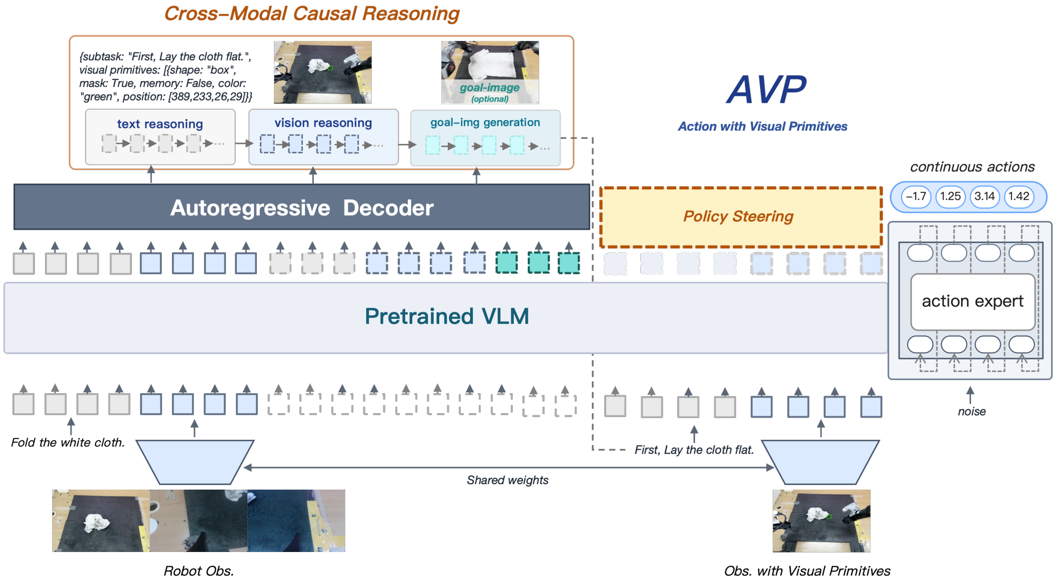

Figure 3: **Overview of the AVP framework.**

4 Experiments

In this section, we evaluate AVP on a suite of real-world robotic manipulation tasks. We first describe the experimental setup and task configurations in section 4.1. We then present quantitative results on multiple manipulation benchmarks in section 4.2. Finally, in section 4.3, we analyze the generalization capability of the proposed method and study the effectiveness of visual primitives.

4.1 Experimental Setup

Task Description. We evaluate our method on three real-world manipulation tasks, including Chinese chess manipulation, domino placement, and general object pick-and-place, as illustrated in fig. 2. The Chinese chess manipulation task serves as the primary benchmark for evaluating spatially precise manipulation. The chessboard contains densely arranged and visually similar chess pieces, posing significant challenges for fine-grained spatial grounding and manipulation accuracy. The domino placement task further evaluates high-precision bimanual manipulation with orientation constraints, requiring accurate target orientation alignment in addition to positional placement. Finally, the general object pick-and-place task evaluates manipulation generalization across objects with diverse visual appearances and geometric shapes.

Dataset, Training, and Evaluation Metrics. We train all policies using real-world expert demonstrations, including 11.2 hours for Chinese chess manipulation, 1.7 hours for domino placement, and 1.7 hours for general object pick-and-place. Our method and the $\pi_{0.5}$ baseline are trained with a batch size of 64; the Chinese chess policy is trained for 40k steps, while the domino and general object policies are trained for 10k steps. Detailed training configurations for other reproduced baselines are provided in the appendix Appendix C. Unless otherwise specified, we report success rates for *Instruction Following*, *Pick Success*, and *Place Success*. Here, *Instruction Following* evaluates whether the policy selects the correct manipulator according to the input instruction. For the domino placement task, we additionally report *Orientation Success* due to its target pose constraints.

Baseline and Robot Embodiment. We build our method on top of the $\pi_{0.5}$ framework and use it as the primary baseline for comparison. Experiments are conducted on an AgileX Piper tabletop platform consisting of two 6-DoF manipulators with parallel grippers. This dual-arm setup defines a unified 14-dimensional action space used for both training and evaluation. Unless otherwise specified, real-robot inference is performed on a single NVIDIA RTX 3090 GPU, and all reported latency measurements are obtained under this setup. For fair comparison, baseline methods are reproduced under the same robot embodiment, training data, and evaluation protocol whenever applicable. For

Method	**Instr.**	**Pick**	**Place**	**Ave.**	**Latency**	**Method**	**Instr.**	**Pick**	**Place**	**Ave.**	**Latency**
$\pi_{0.5}$	74.00	72.00	42.00	62.67	**0.16 s**	DM0	50.00	30.00	15.00	31.67	0.52 s
Point-VLA (Kimi)	65.28	47.22	31.94	48.15	37.32 s	LDA	95.00	20.00	10.00	41.67	0.28 s
Ours	**98.61**	**90.28**	**81.94**	**90.28**	0.27 s	π_0	62.50	45.83	25.00	44.44	**0.16 s**

Table 1: Quantitative evaluation on the Chinese chess manipulation task. All metrics are reported as success rates (%). Ave. denotes the average success rate across all evaluation metrics, and Latency denotes the average inference time per instruction.

Method	Pick	Place	Orien.	Ave.
$\pi_{0.5}$	87.50	**64.58**	93.75	81.94
Ours	**100.00**	**64.58**	**100.00**	**88.19**
Imp.	+12.50	0.00	+6.25	+6.25

Table 2: **Domino placement results.** Metrics are success rates (%).

methods that do not originally support bimanual control, we adapt their action heads to this unified action space while preserving the original model architecture and training protocol as much as possible.

4.2 Main Evaluation

We compare our method with baselines on three real-world manipulation tasks under a unified evaluation protocol.

Experiment I: Chinese chess manipulation. We evaluate the system using a predefined Chinese chess game record, from which we retain 72 non-capture moves for evaluation. To isolate spatial manipulation capabilities, we exclude capture moves; thus, each action simply requires moving a piece from its initial position to a designated target. A move is successful if the piece accurately covers the target board intersection.

To include a baseline based on cascaded visual prompting, we adapt the Point-VLA [19] framework as an additional baseline. While the original Point-VLA uses Claude and Gemini in its visual prompting pipeline, we instantiate the same pipeline with Kimi-K2.5 via Alibaba Cloud Bailian APIs. To further contextualize our results, we include two additional VLA baselines, DM0 [28] and LDA [29]. Due to their extremely long per-step execution time, we evaluate them on a fixed 20-instruction subset and report their results separately from the full 72-instruction evaluation used for all other methods.

As shown in Table 1, our method consistently outperforms all baselines across the evaluation metrics while achieving substantially lower inference latency than cascaded visual prompting methods that rely on online API calls. This highlights its advantage in execution efficiency and real-time deployment.

Experiment II: Domino placement. This task requires the robot to place a domino at a target position with a specified horizontal or vertical orientation. We evaluate the system on 48 instructions against the $\pi_{0.5}$ baseline. A trial is successful if the final position error is within one domino thickness and the angular deviation from the target orientation is under 10°.

As shown in Table 2, the proposed method improves both pick and orientation success rates over the $\pi_{0.5}$ baseline while maintaining comparable placement accuracy. In contrast to the baseline policy, which frequently exhibits repeated grasping and grasp failure behaviors, our method achieves more stable manipulation execution.

Experiment III: General object pick-and-place. This experiment evaluates the proposed method on general object manipulation across diverse object appearances and shapes. As shown in Table 3, the proposed method substantially improves both grasping and placement success rates over the $\pi_{0.5}$ baseline while maintaining perfect correct-manipulator accuracy.

Across all three tasks, the improvements demonstrate the versatility of AVP in real-world manipulation. These results suggest that representing the next-stage target with visual primitives provides

Method	Instr.	Pick	Place	Ave.
$\pi_{0.5}$	**100.00**	71.79	23.08	64.96
Ours	**100.00**	**90.24**	**68.29**	**86.18**
Imp.	0.00	+18.45	+45.21	+21.22

Table 3: **General object manipulation results.** Metrics are success rates (%).

Method	Instr.	Pick	Place	Ave.
$\pi_{0.5}$	0	0	0	0
Ours	**100**	**90**	**60**	**83**

(a) Spatial compositional generalization on unseen direct transitions. Metrics are reported as success rates (%).

Setting	$\pi_{0.5}$	Ours
Chessboard + Direct	0/8	8/8
Chessboard + Indirect	7/8	8/8
White cloth + Direct	0/8	7/8
White cloth + Indirect	0/8	8/8

(b) Cross-domain generalization on representative unseen objects.

Table 4: **Generalization results.** Left: spatial compositional generalization where the model is evaluated on unseen direct board-to-board transitions. Right: zero-shot cross-domain generalization to unseen objects under different background conditions and direct versus indirect execution modes. Results are reported as the number of successfully handled objects out of eight.

a spatially grounded interface between the VLM and the action expert. By separating what-and-where prediction from how-to-execute control, this interface reduces the burden on the action expert and allows it to focus on learning executable motion patterns more efficiently. As a result, AVP achieves improved spatial grounding, manipulation accuracy, and execution stability across diverse real-world settings.

4.3 Generalization and Ablation Studies

We further analyze AVP beyond the main evaluation by studying both its generalization ability and the contribution of visual primitives. We first evaluate whether the visual-primitive interface helps the policy adapt to new spatial configurations and unseen object appearances, rather than overfitting to fixed instruction-action correspondences. We then ablate the visual primitives to assess their role in spatial grounding and manipulation performance. All studies are conducted on the Chinese chess manipulation task from three perspectives: (i) spatial-compositional generalization, (ii) cross-domain generalization to unseen objects, and (iii) visual-primitives ablation.

Spatial-Compositional Generalization. In the training data, all trajectories are decomposed through predefined board-external intermediate waypoints, such that the model only observes two-stage transitions ($A \to C \to B$) and never direct board-to-board transitions ($A \to B$). For this study, we train the model for 50k steps with a batch size of 64 on 12.8 hours of demonstrations, and evaluate it on 50 unseen instructions requiring direct point-to-point execution. This setting evaluates whether the model can compose learned sub-trajectories into novel actions.

As shown in Table 4a, the $\pi_{0.5}$ baseline fails to generalize to unseen direct transitions and cannot produce valid executable actions. In contrast, AVP achieves strong spatial-compositional generalization, suggesting that visual primitives explicitly specify where the robot should act, allowing the action expert to reuse learned motion patterns for unseen spatial configurations.

Cross-Domain Generalization. We further evaluate whether a policy trained solely on Chinese chess manipulation data can generalize to unseen objects in a zero-shot manner. As illustrated in appendix fig. 4, AVP exhibits zero-shot applicability to diverse out-of-domain objects spanning multiple categories. We additionally evaluate under different background conditions and instruction variations. The “Indirect” setting decomposes each move into intermediate seen transitions, following the protocol used in the spatial-compositional generalization study.

As shown in Table 4b, AVP achieves consistently high success rates across unseen objects and background variations. In contrast, the $\pi_{0.5}$ baseline degrades substantially under distribution shifts, particularly in the “Direct” setting. These results suggest that visual primitives improve cross-domain generalization by decoupling motion execution from incidental visual factors such as object appear-

Prompt	Instr.	Pick	Place	Ave.
None	100	70	64	78
Box	100	82	68	83
Box + Mask	100	86	70	85
Box + Mask + Mem.	100	94	78	91

Table 5: **Effect of visual prompt design.** Metrics are reported as success rates (%).

ance and background context. By conditioning the action expert on explicit spatial primitives, AVP allows it to focus on manipulation-relevant geometry, leading to more robust generalization beyond the original Chinese-chess domain. Additional qualitative examples are shown in appendix fig. 5.

Visual Primitives Ablation. We ablate different visual primitive components, including box-based spatial highlighting, background masking, and memory-enhanced primitives. As shown in table 5, box prompts improve manipulation performance, while background masking provides additional gains by suppressing irrelevant visual context. Incorporating memory achieves the best overall performance, suggesting that visual primitives can naturally carry spatial context across manipulation stages. More ablations on visual prompt design are provided in Appendix A.1.

5 Conclusion and Limitations

We presented AVP, an end-to-end VLA architecture that introduces visual primitives as an explicit communication interface between the VLM and the action expert. By decoupling target inference from motion execution, AVP relieves the action expert from implicitly learning spatial grounding from complex multimodal inputs. Crucially, our supervision pipeline derives primitive labels directly from end-effector kinematics, eliminating manual annotation or external perception modules. Real-world experiments across three manipulation tasks demonstrate that AVP consistently outperforms the $\pi_{0.5}$ baseline, achieving an overall success-rate gain of 27.61% alongside strong spatial-compositional generalization.

Despite these advantages, several limitations remain. The sequential, two-stage inference (primitive prediction followed by action generation) introduces additional runtime latency compared to single-pass policies. Furthermore, the supervision pipeline relies on precise hand-eye calibration, which makes the system sensitive to camera extrinsic drifts or physical disturbances.

Acknowledgments

We would like to express our gratitude to Anyverse Dynamics for providing the computing resources, robotic hardware platforms, and technical support that made this work possible.

References

[1] M. J. Kim, K. Pertsch, S. Karamcheti, T. Xiao, A. Balakrishna, S. Nair, R. Rafailov, E. Foster, G. Lam, P. Sanketi, et al. Openvla: An open-source vision-language-action model. *arXiv preprint arXiv:2406.09246*, 2024.

[2] K. Black, N. Brown, D. Driess, A. Esmail, M. Equi, C. Finn, N. Fusai, L. Groom, K. Hausman, B. Ichter, et al. π_0: A vision-language-action flow model for general robot control. *arXiv preprint arXiv:2410.24164*, 2024.

[3] P. Intelligence, K. Black, N. Brown, J. Darpinian, K. Dhabalia, D. Driess, A. Esmail, M. Equi, C. Finn, N. Fusai, et al. $\pi_{0.5}$: a vision-language-action model with open-world generalization. *arXiv preprint arXiv:2504.16054*, 2025.

[4] S. Liu, L. Wu, B. Li, H. Tan, H. Chen, Z. Wang, K. Xu, H. Su, and J. Zhu. Rdt-1b: a diffusion foundation model for bimanual manipulation. *arXiv preprint arXiv:2410.07864*, 2024.

[5] O. M. Team, D. Ghosh, H. Walke, K. Pertsch, K. Black, O. Mees, S. Dasari, J. Hejna, T. Kreiman, C. Xu, et al. Octo: An open-source generalist robot policy. *arXiv preprint arXiv:2405.12213*, 2024.

[6] O. X.-E. Collaboration, A. O'Neill, A. Rehman, A. Gupta, A. Maddukuri, A. Gupta, A. Padalkar, A. Lee, A. Pooley, A. Gupta, A. Mandlekar, A. Jain, A. Tung, A. Bewley, A. Herzog, A. Irpan, A. Khazatsky, A. Rai, A. Gupta, A. Wang, A. Kolobov, A. Singh, A. Garg, A. Kembhavi, A. Xie, A. Brohan, A. Raffin, A. Sharma, A. Yavary, A. Jain, A. Balakrishna, A. Wahid, B. Burgess-Limerick, B. Kim, B. Schölkopf, B. Wulfe, B. Ichter, C. Lu, C. Xu, C. Le, C. Finn, C. Wang, C. Xu, C. Chi, C. Huang, C. Chan, C. Agia, C. Pan, C. Fu, C. Devin, D. Xu, D. Morton, D. Driess, D. Chen, D. Pathak, D. Shah, D. Büchler, D. Jayaraman, D. Kalashnikov, D. Sadigh, E. Johns, E. Foster, F. Liu, F. Ceola, F. Xia, F. Zhao, F. V. Frujeri, F. Stulp, G. Zhou, G. S. Sukhatme, G. Salhotra, G. Yan, G. Feng, G. Schiavi, G. Berseth, G. Kahn, G. Yang, G. Wang, H. Su, H.-S. Fang, H. Shi, H. Bao, H. B. Amor, H. I. Christensen, H. Furuta, H. Bharadhwaj, H. Walke, H. Fang, H. Ha, I. Mordatch, I. Radosavovic, I. Leal, J. Liang, J. Abou-Chakra, J. Kim, J. Drake, J. Peters, J. Schneider, J. Hsu, J. Vakil, J. Bohg, J. Bingham, J. Wu, J. Gao, J. Hu, J. Wu, J. Wu, J. Sun, J. Luo, J. Gu, J. Tan, J. Oh, J. Wu, J. Lu, J. Yang, J. Malik, J. Silvério, J. Hejna, J. Booher, J. Tompson, J. Yang, J. Salvador, J. J. Lim, J. Han, K. Wang, K. Rao, K. Pertsch, K. Hausman, K. Go, K. Gopalakrishnan, K. Goldberg, K. Byrne, K. Oslund, K. Kawaharazuka, K. Black, K. Lin, K. Zhang, K. Ehsani, K. Lekkala, K. Ellis, K. Rana, K. Srinivasan, K. Fang, K. P. Singh, K.-H. Zeng, K. Hatch, K. Hsu, L. Itti, L. Y. Chen, L. Pinto, L. Fei-Fei, L. Tan, L. J. Fan, L. Ott, L. Lee, L. Weihs, M. Chen, M. Lepert, M. Memmel, M. Tomizuka, M. Itkina, M. G. Castro, M. Spero, M. Du, M. Ahn, M. C. Yip, M. Zhang, M. Ding, M. Heo, M. K. Srirama, M. Sharma, M. J. Kim, M. Z. Irshad, N. Kanazawa, N. Hansen, N. Heess, N. J. Joshi, N. Suenderhauf, N. Liu, N. D. Palo, N. M. M. Shafiullah, O. Mees, O. Kroemer, O. Bastani, P. R. Sanketi, P. T. Miller, P. Yin, P. Wohlhart, P. Xu, P. D. Fagan, P. Mitrano, P. Sermanet, P. Abbeel, P. Sundaresan, Q. Chen, Q. Vuong, R. Rafailov, R. Tian, R. Doshi, R. Mart'in-Mart'in, R. Baijal, R. Scalise, R. Hendrix, R. Lin, R. Qian, R. Zhang, R. Mendonca, R. Shah, R. Hoque, R. Julian, S. Bustamante, S. Kirmani, S. Levine, S. Lin, S. Moore, S. Bahl, S. Dass, S. Sonawani, S. Tulsiani, S. Song, S. Xu, S. Haldar, S. Karamcheti, S. Adebola, S. Guist, S. Nasiriany, S. Schaal, S. Welker, S. Tian, S. Ramamoorthy, S. Dasari, S. Belkhale, S. Park, S. Nair, S. Mirchandani, T. Osa, T. Gupta, T. Harada, T. Matsushima, T. Xiao, T. Kollar, T. Yu, T. Ding, T. Davchev, T. Z. Zhao, T. Armstrong, T. Darrell, T. Chung, V. Jain, V. Kumar, V. Vanhoucke,

V. Guizilini, W. Zhan, W. Zhou, W. Burgard, X. Chen, X. Chen, X. Wang, X. Zhu, X. Geng, X. Liu, X. Liangwei, X. Li, Y. Pang, Y. Lu, Y. J. Ma, Y. Kim, Y. Chebotar, Y. Zhou, Y. Zhu, Y. Wu, Y. Xu, Y. Wang, Y. Bisk, Y. Dou, Y. Cho, Y. Lee, Y. Cui, Y. Cao, Y.-H. Wu, Y. Tang, Y. Zhu, Y. Zhang, Y. Jiang, Y. Li, Y. Li, Y. Iwasawa, Y. Matsuo, Z. Ma, Z. Xu, Z. J. Cui, Z. Zhang, Z. Fu, and Z. Lin. Open X-Embodiment: Robotic learning datasets and RT-X models. `https://arxiv.org/abs/2310.08864`, 2023.

[7] A. Khazatsky, K. Pertsch, S. Nair, A. Balakrishna, S. Dasari, S. Karamcheti, S. Nasiriany, M. K. Srirama, L. Y. Chen, K. Ellis, P. D. Fagan, J. Hejna, M. Itkina, M. Lepert, Y. J. Ma, P. T. Miller, J. Wu, S. Belkhale, S. Dass, H. Ha, A. Jain, A. Lee, Y. Lee, M. Memmel, S. Park, I. Radosavovic, K. Wang, A. Zhan, K. Black, C. Chi, K. B. Hatch, S. Lin, J. Lu, J. Mercat, A. Rehman, P. R. Sanketi, A. Sharma, C. Simpson, Q. Vuong, H. R. Walke, B. Wulfe, T. Xiao, J. H. Yang, A. Yavary, T. Z. Zhao, C. Agia, R. Baijal, M. G. Castro, D. Chen, Q. Chen, T. Chung, J. Drake, E. P. Foster, J. Gao, V. Guizilini, D. A. Herrera, M. Heo, K. Hsu, J. Hu, M. Z. Irshad, D. Jackson, C. Le, Y. Li, K. Lin, R. Lin, Z. Ma, A. Maddukuri, S. Mirchandani, D. Morton, T. Nguyen, A. O'Neill, R. Scalise, D. Seale, V. Son, S. Tian, E. Tran, A. E. Wang, Y. Wu, A. Xie, J. Yang, P. Yin, Y. Zhang, O. Bastani, G. Berseth, J. Bohg, K. Goldberg, A. Gupta, A. Gupta, D. Jayaraman, J. J. Lim, J. Malik, R. Martín-Martín, S. Ramamoorthy, D. Sadigh, S. Song, J. Wu, M. C. Yip, Y. Zhu, T. Kollar, S. Levine, and C. Finn. Droid: A large-scale in-the-wild robot manipulation dataset. 2024.

[8] H. Walke, K. Black, A. Lee, M. J. Kim, M. Du, C. Zheng, T. Zhao, P. Hansen-Estruch, Q. Vuong, A. He, V. Myers, K. Fang, C. Finn, and S. Levine. Bridgedata v2: A dataset for robot learning at scale. In *Conference on Robot Learning (CoRL)*, 2023.

[9] H. Geng, F. Wang, S. Wei, Y. Li, B. Wang, B. An, C. T. Cheng, H. Lou, P. Li, Y.-J. Wang, et al. Roboverse: Towards a unified platform, dataset and benchmark for scalable and generalizable robot learning. *arXiv preprint arXiv:2504.18904*, 2025.

[10] B. Zitkovich, T. Yu, S. Xu, P. Xu, T. Xiao, F. Xia, J. Wu, P. Wohlhart, S. Welker, A. Wahid, et al. Rt-2: Vision-language-action models transfer web knowledge to robotic control. In *Conference on Robot Learning*, pages 2165–2183. PMLR, 2023.

[11] J. Zhang, X. Chen, Q. Wang, M. Li, Y. Guo, Y. Hu, J. Zhang, S. Bai, J. Lin, and J. Chen. Vlm4vla: Revisiting vision-language-models in vision-language-action models. *arXiv preprint arXiv:2601.03309*, 2026.

[12] N. Kachaev, M. Kolosov, D. Zelezetsky, A. K. Kovalev, and A. I. Panov. Don't blind your vla: Aligning visual representations for ood generalization. *arXiv preprint arXiv:2510.25616*, 2025.

[13] A. J. Hancock, X. Wu, L. Zha, O. Russakovsky, and A. Majumdar. Actions as language: Fine-tuning vlms into vlas without catastrophic forgetting. *arXiv preprint arXiv:2509.22195*, 2025.

[14] S. Belkhale, T. Ding, T. Xiao, P. Sermanet, Q. Vuong, J. Tompson, Y. Chebotar, D. Dwibedi, and D. Sadigh. Rt-h: Action hierarchies using language. *arXiv preprint arXiv:2403.01823*, 2024.

[15] L. X. Shi, B. Ichter, M. Equi, L. Ke, K. Pertsch, Q. Vuong, J. Tanner, A. Walling, H. Wang, N. Fusai, et al. Hi robot: Open-ended instruction following with hierarchical vision-language-action models. *arXiv preprint arXiv:2502.19417*, 2025.

[16] P. Intelligence, B. Ai, A. Amin, R. Aniceto, A. Balakrishna, G. Balke, K. Black, et al. $\pi_{0.7}$: A steerable generalist robotic foundation model with emergent capabilities. *arXiv preprint arXiv:2604.15483*, 2026.

[17] S. Gao, J. Yang, L. Chen, K. Chitta, Y. Qiu, A. Geiger, J. Zhang, and H. Li. Vista: A generalizable driving world model with high fidelity and versatile controllability. *arXiv preprint arXiv:2405.17398*, 2024.

[18] T. Yuan, Z. Dong, Y. Liu, and H. Zhao. Fast-wam: Do world action models need test-time future imagination? *arXiv preprint arXiv:2603.16666*, 2026.

[19] H. Yu, J. Zhao, Y. Liu, K. Li, C. Ma, D. Zhang, Y. Hu, G. Chen, J. Xie, J. Guo, et al. Point what you mean: Visually grounded instruction policy. *arXiv preprint arXiv:2512.18933*, 2025.

[20] Z. Wang, Y. Chen, Y. Liu, J. Ye, P. Chen, C. Lu, S. Liu, and J. Jia. Vp-vla: Visual prompting as an interface for vision-language-action models. *arXiv preprint arXiv:2603.22003*, 2026.

[21] R. Zheng, Y. Liang, S. Huang, J. Gao, H. Daumé III, A. Kolobov, F. Huang, and J. Yang. Tracevla: Visual trace prompting enhances spatial-temporal awareness for generalist robotic policies. *arXiv preprint arXiv:2412.10345*, 2024.

[22] H. Wu, Y. Jing, C. Cheang, G. Chen, J. Xu, X. Li, M. Liu, H. Li, and T. Kong. Unleashing large-scale video generative pre-training for visual robot manipulation, 2023.

[23] C.-L. Cheang, G. Chen, Y. Jing, T. Kong, H. Li, Y. Li, Y. Liu, H. Wu, J. Xu, Y. Yang, H. Zhang, and M. Zhu. Gr-2: A generative video-language-action model with web-scale knowledge for robot manipulation. *arXiv preprint arXiv:2410.06158*, 2024.

[24] A. Brohan, N. Brown, J. Carbajal, Y. Chebotar, J. Dabis, C. Finn, K. Gopalakrishnan, K. Hausman, A. Herzog, J. Hsu, et al. Rt-1: Robotics transformer for real-world control at scale. *arXiv preprint arXiv:2212.06817*, 2022.

[25] C. Cheang, S. Chen, Z. Cui, Y. Hu, L. Huang, T. Kong, H. Li, Y. Li, Y. Liu, X. Ma, et al. Gr-3 technical report. *arXiv preprint arXiv:2507.15493*, 2025.

[26] C. Chi, S. Feng, Y. Du, Z. Xu, E. Cousineau, B. Burchfiel, and S. Song. Diffusion policy: Visuomotor policy learning via action diffusion. In *Proceedings of Robotics: Science and Systems (RSS)*, 2023.

[27] C. Chi, Z. Xu, S. Feng, E. Cousineau, Y. Du, B. Burchfiel, R. Tedrake, and S. Song. Diffusion policy: Visuomotor policy learning via action diffusion. *The International Journal of Robotics Research*, 2024.

[28] E. Yu et al. Dm0: An embodied-native vision-language-action model towards physical ai. *arXiv preprint arXiv:2602.14974*, 2026.

[29] J. Chen et al. Lda-1b: Scaling latent dynamics action model via universal embodied data ingestion. *arXiv preprint arXiv:2602.12215*, 2026.

[30] T. Lin, G. Li, Y. Zhong, Y. Zou, Y. Du, J. Liu, E. Gu, and B. Zhao. Evo-0: Vision-language-action model with implicit spatial understanding. *arXiv preprint arXiv:2507.00416*, 2025.

[31] S. Fei, S. Wang, J. Shi, Z. Dai, J. Cai, P. Qian, L. Ji, X. He, S. Zhang, Z. Fei, J. Fu, J. Gong, and X. Qiu. Libero-plus: In-depth robustness analysis of vision-language-action models. *arXiv preprint arXiv:2510.13626*, 2025.

[32] G. R. Team, S. Abeyruwan, J. Ainslie, J.-B. Alayrac, M. G. Arenas, T. Armstrong, A. Balakrishna, R. Baruch, M. Bauza, M. Blokzijl, et al. Gemini robotics: Bringing ai into the physical world. *arXiv preprint arXiv:2503.20020*, 2025.

[33] N. Ravi, V. Gabeur, Y.-T. Hu, R. Hu, C. Ryali, T. Ma, H. Khedr, R. Rädle, C. Rolland, L. Gustafson, et al. Sam 2: Segment anything in images and videos. *arXiv preprint arXiv:2408.00714*, 2024.

[34] N. Carion, L. Gustafson, Y.-T. Hu, S. Debnath, R. Hu, D. Suris, C. Ryali, K. V. Alwala, H. Khedr, A. Huang, et al. Sam 3: Segment anything with concepts. *arXiv preprint arXiv:2511.16719*, 2025.

[35] G. Team, R. Anil, S. Borgeaud, J.-B. Alayrac, J. Yu, R. Soricut, J. Schalkwyk, A. M. Dai, A. Hauth, K. Millican, et al. Gemini: a family of highly capable multimodal models. *arXiv preprint arXiv:2312.11805*, 2023.

[36] J. Achiam, S. Adler, S. Agarwal, L. Ahmad, I. Akkaya, F. L. Aleman, D. Almeida, J. Altenschmidt, S. Altman, S. Anadkat, et al. Gpt-4 technical report. *arXiv preprint arXiv:2303.08774*, 2023.

[37] H. Liu, C. Li, Q. Wu, and Y. J. Lee. Visual instruction tuning, 2023.

[38] K. Fang, F. Liu, P. Abbeel, and S. Levine. Moka: Open-world robotic manipulation through mark-based visual prompting. *Robotics: Science and Systems (RSS)*, 2024.

[39] X. Li, L. Xu, M. Zhang, J. Liu, Y. Shen, I. Ponomarenko, J. Xu, L. Heng, S. Huang, S. Zhang, et al. Crayonrobo: Object-centric prompt-driven vision-language-action model for robotic manipulation. *arXiv preprint arXiv:2505.02166*, 2025.

[40] W. Huang, C. Wang, Y. Li, R. Zhang, and L. Fei-Fei. Rekep: Spatio-temporal reasoning of relational keypoint constraints for robotic manipulation. *arXiv preprint arXiv:2409.01652*, 2024.

[41] S. Huang, H. Chang, Y. Liu, Y. Zhu, H. Dong, P. Gao, A. Boularias, and H. Li. A3vlm: Actionable articulation-aware vision language model. *arXiv preprint arXiv:2406.07549*, 2024.

[42] Z. Qi, W. Zhang, Y. Ding, R. Dong, X. Yu, J. Li, L. Xu, B. Li, X. He, G. Fan, et al. Sofar: Language-grounded orientation bridges spatial reasoning and object manipulation. *arXiv preprint arXiv:2502.13143*, 2025.

[43] H. Liu, S. Guo, P. Mai, J. Cao, H. Li, and J. Ma. Robodexvlm: Visual language model-enabled task planning and motion control for dexterous robot manipulation. In *2025 IEEE/RSJ International Conference on Intelligent Robots and Systems (IROS)*, pages 1381–1388. IEEE, 2025.

[44] T. Dai, M. Han, T. Du, Z. Liu, Z. Li, S. Khan, J. Yu, and X. Chang. See, plan, rewind: Progress-aware vision-language-action models for robust robotic manipulation. *arXiv preprint arXiv:2603.09292*, 2026.

[45] Y. Li, Z. Gong, H. Li, X. Huang, H. Kang, G. Bai, and X. Ma. Robotic visual instruction. 2025.

A Additional Experimental Results

A.1 Visual Primitives Ablation

We conduct additional ablation studies to analyze the impact of different visual primitives designs on manipulation performance. Specifically, we investigate (i) primitives types and (ii) mask opacity.

All experiments are conducted using 25,282.7 seconds of training data for 10k steps, and evaluated on 50 instructions from the main evaluation benchmark.

Visual Primitive Type. We compare four types of visual primitives: *raw* (no prompt), *point*, *box*, and *box-mask*. Results are summarized in Table 6.

Prompt Type	Instr.	Pick	Place
Raw	100	70	64
Point	100	86	74
Box	100	82	68
Box-mask	100	86	70

Table 6: **Effect of visual prompt types.**

Mask Opacity. We further analyze the effect of mask opacity in the box-mask setting. Results are summarized in Table 7.

Opacity	Instr.	Pick	Place
$\alpha = 0$	100	82	68
$\alpha = 0.7$	100	86	70
$\alpha = 0.9$	100	86	74

Table 7: **Effect of mask opacity in box-mask prompts.**

Discussion. Introducing visual prompts significantly improves performance compared to the raw setting, confirming the importance of spatial grounding. Among different prompt types, point and box-mask achieve stronger performance, while mask opacity mainly affects placement accuracy. These results suggest that precise spatial highlighting is beneficial for manipulation.

A.2 Visualization of Cross-Domain Generalization results

We provide further qualitative visualizations of our zero-shot cross-domain generalization experiments in fig. 5. As shown, the leftmost column displays a diverse set of unseen, out-of-distribution (OOD) test objects, while the subsequent columns depict the successful continuous grasping trajectories executed by AVP. While the $\pi_{0.5}$ baseline exhibits severe degradation under such distribution shifts, our method maintains remarkable robustness. By leveraging explicit visual prompts as an intermediate representation, AVPeffectively decouples spatial control from specific object semantics, enabling the emergence of highly transferable, object-agnostic manipulation skills.

B Details of Action-Centric Visual-Primitive Supervision

This section provides full details of the proposed action-centric visual-primitive supervision pipeline. Our goal is to construct reliable primitive labels directly from robot interaction trajectories, avoiding the semantic ambiguity and maintenance cost of external perception-based annotation pipelines.

Overview. We decompose the supervision construction process into three sequential stages: (i) kinematic keyframe extraction, (ii) spatial pose estimation, and (iii) discretized primitive projection. The key principle is to determine *when* interaction occurs from robot kinematics and *where* the corresponding primitive should be spatially grounded via geometric projection.

Figure 4: **OOD object gallery for cross-domain generalization.** We evaluate zero-shot transfer on 45 unseen objects spanning multiple categories beyond the Chinese chess training domain.

Kinematic keyframe extraction. We first identify critical interaction keyframes by detecting substantial transitions in the gripper state. Let g_t denote the gripper state signal at time step t, such as the discrepancy between the gripper control command and the measured physical aperture. We define the interaction keyframe set as

$$T_{\text{key}} = \{\, t \in [1, T] \mid |\Delta g_t| > \delta \,\}, \tag{7}$$

where δ is a predefined threshold for detecting significant gripper state transitions. Intuitively, these keyframes correspond to physically meaningful interaction events such as grasp initiation or release.

Spatial pose estimation. For each keyframe $t \in T_{\text{key}}$, we extract the corresponding 3D end-effector position

$$P_t = [X_t, Y_t, Z_t]^T \in \mathbb{R}^3 \tag{8}$$

from robot proprioception. This position provides a physically grounded estimate of the interaction location in the robot base coordinate frame.

Primitive projection. We then project the 3D interaction point into the image plane to obtain a 2D spatial anchor $m_t = (u_t, v_t)$. Let $K \in \mathbb{R}^{3\times 3}$ denote the camera intrinsic matrix, and let $T_R^C \in SE(3)$ denote the extrinsic transformation from the robot base frame to the camera frame. The projected image coordinate is computed via standard perspective projection:

$$z_c \begin{bmatrix} u_t \\ v_t \\ 1 \end{bmatrix} = K T_R^C \begin{bmatrix} P_t \\ 1 \end{bmatrix}, \tag{9}$$

where z_c is the depth scaling factor in the camera coordinate system. The resulting 2D point (u_t, v_t) serves as the spatial anchor for constructing the primitive label.

Discretized primitive construction. Given the projected anchor (u_t, v_t), we discretize its image-plane location into a finite spatial grid to obtain the supervision target for the visual-primitive decoder. Compared with primitive labels generated by generic perception models, these anchors are directly aligned with the underlying physical interaction trajectory and therefore provide more reliable spatial grounding for manipulation learning.

Discussion. This kinematics-guided supervision process offers two main advantages. First, it avoids the semantic ambiguity of external perception pipelines, especially in settings with visually similar objects, occlusion, or cluttered scenes. Second, it significantly reduces annotation cost

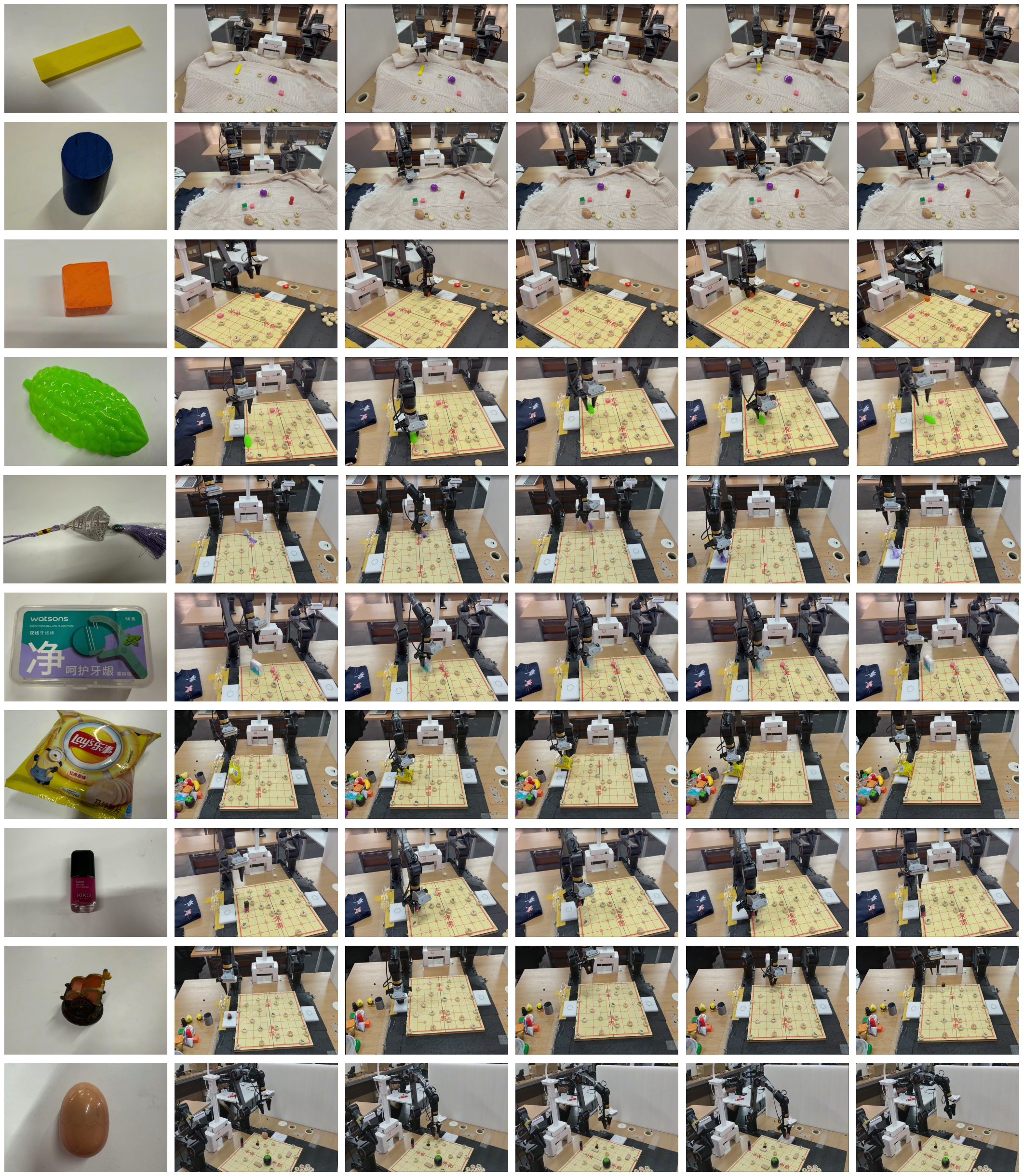

Figure 5: **Qualitative results for zero-shot cross-domain generalization.** The leftmost column displays unseen OOD test objects, and the right columns illustrate the successful grasping trajectories executed by AVP.

by replacing manual or model-based primitive generation with an automated geometric pipeline. As a result, it provides a scalable and physically grounded supervision source for training the proposed visual-primitive interface.

C Training Details of Baselines

For reproduced baselines, training steps are selected to ensure stable optimization and near-converged performance under their respective implementations. In particular, DM0 and LDA require more training steps than $\pi_{0.5}$ and our method to reach stable convergence in our bimanual setting. We therefore report task-specific training configurations that aim to provide each baseline with a fair and sufficiently optimized comparison setting, rather than enforcing identical step counts across methods.

Table 8: Training configurations for reproduced baselines.

Method	Batch Size	Training Steps
$\pi_{0.5}$ / Point-VLA / Ours	64	40k (Chinese chess), 10k (domino/general object)
DM0	32	50k
LDA	32	50k (until convergence)